



Experimental Study for Evaluating the Efficiency of Nanocomposites Materials for Biomicrite Limestone Consolidation

Mohsen M. Saleh^{a*}, S. H. M. Alagamawy^b, Ahmed N. Emam^{c,d}

^a Conservation Dept. Faculty of Archaeology, Cairo University, Giza, Egypt

^b postgraduate student, Conservation Dept. Faculty of Archeology, Cairo University, chemical researcher at the Radio Engineering Research Center in El Haram

^c Refractories, Ceramics and Building Materials Department, Advanced Material Technology & Mineral Resources Research Institute, National Research Centre (NRC), El Bohouth St., Dokki, 12622 Cairo, Egypt

^d Nanomedicine & Tissue Engineering Research Lab, Medical Research Centre of Excellence, National Research Centre, El Bohouth St., Dokki, 12622 Cairo, Egypt



Abstract

Biomicrite is one of the most common types of limestone used in archaeological architecture, such as the Cairo Citadel Aqueduct, and it is organic carbonate sedimentary rock, as microfossils and metabolic residues of extinct animals are filled with fine-grained calcite and/or dolomite are scattered in the very fine-grained matrix (micrite), which makes it a relatively weak sedimentary stone, and its preservation is a difficult challenge facing conservators, so they resort to using compatible consolidate materials with limestone components. Nanocomposites are a recent trend in the treatment and conservation of monuments, as they aim to perform a number of functions at the same time, with minimal external chemicals interference. This experimental study aims to evaluate the efficiency of a number of multifunctional nanocomposites, namely nano zinc titanate added to nano barium hydroxide or nano barium titanate or nano barium oxide mixed in paraloid B-72 dissolved in high purity acetone, by examining the consolidate stones samples using stereo microscope, PM, SEM, XRD and water contact angle, in addition to measuring the mechanical properties and colorimetric measurement, it was found that nano zinc titrate added to nano barium oxide mixed with paraloid B-72 dissolved in high pure acetone gave the best results.

Keywords: physical and mechanical properties, PM, XRD, SEM, contact angle, colorimetric measurement, nano BaO

1. Introduction

Limestone is a widespread building material in Egypt, where it has been used since the ancient Egyptian civilization -the Third Dynasty, Old Kingdom - until today (Shoaib Ahmed, Kamal Heba, 2020, 1) (Bourguignon, 2000, 17) was quarried in geological formations dating from the Paleocene especially the Eocene epoch of the Paleocene period (Al-Dosari, et al, 2017, 2). Cairo Citadel Aqueduct is considered one of the most unique monuments built of limestone taken from the Mokattam quarries (Saleh Mohsen M., et al., 2022), due to the fact that it

is one of the building stones exposed to different environmental conditions, and the conservation of such types of open-air limestone always represents a complex task (Griffin et al. 1991, 194). Therefore, conservators always seek to use conservation materials and techniques with the aim of not only preserving the current state of exposed limestone but also achieving future preventive effects. Where Cairo Citadel Aqueduct is one of the Ayyubid monuments that are distinguished for being built with limestone is of a similar nature, in terms of the geological

* Corresponding author: E-mail addresses: mohsen_saleh@cu.edu.eg / mohsensaleh_22@yahoo.com., (Mohsen M. Saleh)

EJCHEM use only: Received date 27 April 2023; revised date 16 May 2023; accepted date 30 May 2023

DOI: 10.21608/EJCHEM.2023.207628.7910

©2023 National Information and Documentation Center (NIDOC)

composition, and the damage they suffer from, due to the similar conditions of their existence and the factors affecting them. Egyptian limestone is considered to be vulnerable to weathering compared with other limestones; the arid climate of Cairo only serves to exacerbate the deterioration of the naturally susceptible Egyptian stone. Deterioration processes, are generally detrimental to any stone's ability to reduce the integrity of the masonry structure, are particularly harmful in such an inherently weak limestone (McCormack, 2001, 9) (Fitzner et al., 2002).

Nanotechnology is one of the modern techniques used in restoration and conservation of monuments, whether fixed or movable, which included a number of different treatment processes such as cleaning, strengthening, completion, assembly and sterilization, in addition to various preventive conservation process from inhibiting microbiological growths, self-cleaning and protection from the influence of both ultraviolet rays and moisture (Abu Karora, 2018) (Giorgi et al., 2002) (Perez, 2019), the materials, that were included in these processes varied according to the type of process to be carried out, and the type of antiquity material to which it will be applied. The processes of consolidation in limestone using nanomaterials have been studied, as they are characterized by their small size, which enables them to penetrate quickly and deeply into the stone material, and increase their interacting surfaces, which improves the mechanical and chemical properties of the materials treated with them, without affecting the archaeological surface (Baglioni, et al., 2014) (Baglioni Piero, Giorgi Rodorico, 2006) (David, et al., 2020) (Ion, et al., 2017) (Waked, 2011) (Ferrari, et al., 2015). In recent years reinforcement of nano silica (SiO_2), nanomaterials such as nano titania (TiO_2) and nanoalumina (Al_2O_3) have been studied as insulating materials, which have achieved good results. Despite the success of nano copper oxide (CuO) as an inhibitor of microbiological growth, it has been shown by chromatic measurements - darken of color - and thus its exclusion in the treatment of archaeological materials (Ruffolo, La Russa, 2019).

In the field of self-cleaning, use of nano-titanium oxide (TiO_2) in the work of self-protection for a number of materials, so it was mixed with paraloid B44, as it gave a dense and homogeneous protective layer on the surface without a complete closure of the

pores, and it did not cause color change, and it proved effective It is great at eliminating fungal growth, resisting the treated surface from sanding, and expelling dust (Ahmed Sayed, 2014). In the field of consolidation, used nano calcium hydroxide [$\text{Ca}(\text{OH})_2$], and nan silica (SiO_2), found that it was super hydrophobic and photocatalytic, and since dirt and early colonies of microorganisms do not adhere to the surface itself, and are generally 'washed away' by water, being highly hydrophobic, it preserved the lithic archaeological material from the corrosive effect of water. Conversely, photoactive surfactant organic matter can adhere to the surface, which can be easily oxidized via photocatalysis of nanomaterials (Baglioni, Giorgi, 2006) (Rodriguez-Navarro, Ruiz-Agudo, 2017) (Pozo-Antonio et al., 2019).

Crystalline titanium dioxide is the most widely used photocatalyst for curing stone monuments, but other metal oxide nanoparticles have also been used, and zinc and titanium oxide (ZnTiO_3) and cupric oxide (CuO), which gave similar results in terms of self-cleaning and biocidal efficacy. Conducted other experiments by adding catalysts (doping) to nanotitania such as silver (Ag), copper (Cu), gold (Au), and nitrogen (N). Catalysis by inserting atoms of these elements into the crystal lattice of nanotitania. In some cases the metal does not enter the crystal lattice, but is located on the surface of the nanoparticles. This process can generate variation in the photoactivity of titania nanoparticles. Some Silver Catalysis Titanium nanoparticles have a strong effect as a microbial growth inhibitor, also due to the antimicrobial feature of silver itself. The main disadvantage of stimulation with elements is chromatic aberration, such stimulation may lead to absorption in the visible region of electromagnetic radiation, so this coating can cause strong and unacceptable chromatic aberrations on the treated surface. (Ruffolo, La Russa, 2019)

Multifunctional nanocomposites are a new technique used in the field of restoration and conservation of antiquities, given that the nanocomposites contain more than one nanomaterial present in alloy form which improves the physical or chemical properties (Sen Mousumi, 2020) and allow less chemical interference on the antiquities, which is encouraged by protocols for preserving antiquities. In this study, some nanocomposites materials efficiency was evaluated for limestone treatment.

2. Materials and Methods

2.1. Materials

Zinc acetate dihydrate ($\text{Zn}(\text{CH}_3\text{COO})_2 \cdot 2\text{H}_2\text{O}$, 99%, Chem-Lab, Belgium); Titanium(IV) isoperoxide ($\text{Ti}[\text{OCH}(\text{CH}_3)_2]_4$, Titanium as $\text{TiO}_2 \sim 27.5 - 28.5\%$, Advent CHEMBIO PVT. LTD., India); Barium chloride dihydrate ($\text{BaCl}_2 \cdot 2\text{H}_2\text{O}$, 99% Sigma Aldrich, Germany); Sodium Hydroxide Pellets (NaOH , 99%, Nasr Chemicals, Egypt); 2-Propanol ($(\text{CH}_3)_2\text{CHOH}$, 85-99%, Sd-Fine Chemicals); Ethanol absolute ($\text{CH}_3\text{CH}_2\text{OH}$, 99%, Sigma Aldrich, Germany), and doubled distilled water

2.2. Sample preparation

Limestone samples have been taken from the quarries of Tura, since it is the source of the stones of Cairo Citadel Aqueduct, Tura quarries are located about 15 km north of Cairo (Shoaib Ahmed, Kamal Heba, 2020, 2). After bringing the limestone tiles they were cut into small cubes ($3 \times 3 \times 3 \text{ cm}^3$) (ASTM C97/C97M – 2015), which were divided into two standard groups, the first one coded by 'bg', which is pre-aging samples, and the second group coded by 'ag' which are aging samples, and three groups coded by 'a, b, and c' in which nanomaterials are applied to one of its surfaces to evaluate it (Fig.1), that groups of sample 'ag and bg' each one has 6 cubes, where groups of sample 'a, b, and c' each one has 12 cubes totally 48 cubes, and for mechanical properties of standard group 'bg' small cubes have volume ($5 \times 5 \times 5 \text{ cm}^3$) (ASTM C170/C170M– 2015)

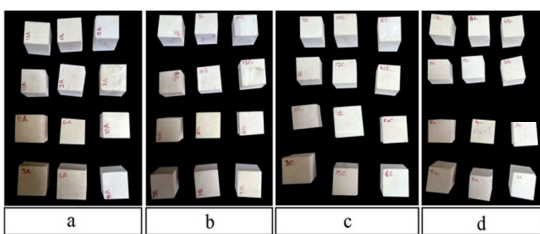


Fig. 1 (a): Treated samples, group 'a', (b) Treated samples group 'b', (c) treated samples, group 'c', and (d) untreated samples, groups 'bg = before aging (standard)''

The groups 'ag, a, b, and c' were aged according to ASTM D5240/ D5240M- 2013, then the different nanocomposites mixture were applied to groups 'a, b, and c' using brushes, where 3% of Nanocomposites mixture added to 2% Paraloid B-72 soluble in high pure Acetone (98%). The Nanocomposites are zinc titanate (ZnTiO_3) mixed with, group 'a' barium hydroxide $\text{Ba}(\text{OH})_2$, group 'b' barium titanate (BaTiO_3), and group 'c' barium oxide (BaO)

2.3. Procedure of Thermal drought cycles according to ASTM D5240/ D5240M- 2013:

- 1- Describe each slab as indicated in Practice D 5121.
- 2- Dry each slab in an oven to a constant mass at $110 \pm 5^\circ\text{C}$ ($230 \pm 9^\circ\text{F}$), and record the mass. In most cases, drying slabs overnight (12 to 16 h) is sufficient. In cases where there is doubt concerning the adequacy of drying, drying should be continued until the change in mass after two time intervals (greater than 1 h) of drying is less than about 1 %.
- 3- Place each slab in an individual basket and immerse it in a sulfate solution, according to the procedure of 9 of Test Method C 88.
- 4- Repeat the process of immersion and drying for a total of five cycles.

After completely dry the group samples 'a, b, and c', the second aging was applied, but samples cannot withstand the aging cycle, so it began to collapse and deteriorate after the first salt weathering cycles, while it was in good condition in the thermal drought cycles (Fig.2)

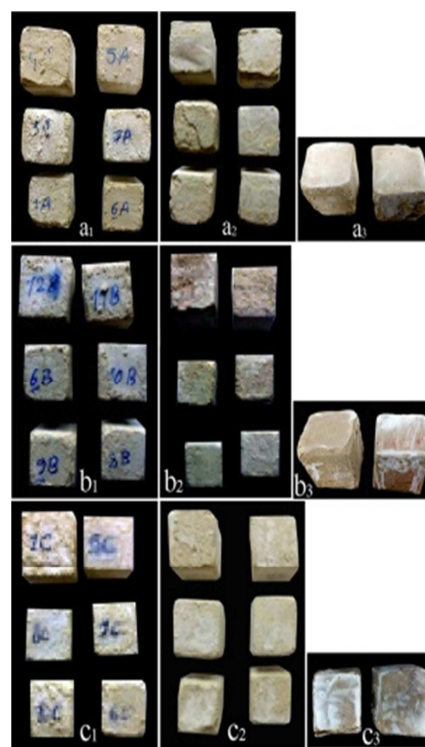


Fig. 2: Different types of deterioration decay to samples after second aging, (a1-a3) samples group "a", (b1-b3) samples group "b" and (c1-c3) samples group "c"

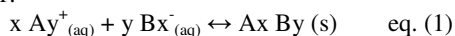
2.4. Rational for using selected nanomaterials

In this study, a mixture of Zinc titanate (ZnTiO_3) as a base material was embedded in polymeric matrix B72 which is composed of ethyl methacrylate (70%) and methyl acrylate (30%) copolymer. In such case, (ZnTiO_3) supposed to have superior self-cleaning, UV block, and antimicrobial activity (Ruffolo, et al, 2010). Where ZnO (1st ingredient of nano-alloy) have ability to increase the split tensile and flexural strengths. In addition, ZnO NPs supposed to improve the pore structure and mechanical strength of limestone as well in concrete. While the 2nd counterpart of obtained nano-alloy (i.e., TiO_2) have a superior self-cleaning, antimicrobial and photocatalytic activity that contribute to save the limestone surface from the ambient pollution, such as, (CO_2), organic dyes and bio-film (Balboul, et al, 2019) (Licciulli, et al, 2011) (Goffredo, et al., 2014) (Sassoni, et al., 2018).

On the other hand, barium hydroxide (Ba(OH)_2), barium titanate (BaTiO_3) and barium oxide (BaO) has been used as supporting materials; Barium hydroxide (Ba(OH)_2) and Barium oxide have a long history as a potential consolidant for stone (Rodrigues, Pinto, 2015) (Karatasios, 2005). It is based on the idea that the product once inside the stone it precipitates as barium hydroxide that converts to barium carbonate by the action of the atmospheric (CO_2), with a possible complementary mechanism in the case of calcite and dolomite substrates.

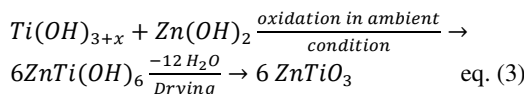
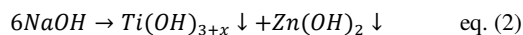
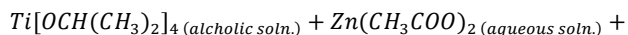
2.5. Fabrication Approaches for selected nanomaterials

In the current study, all of suggested nanomaterials have been prepared via co-precipitation chemical routes. Co-precipitation reactions involve the simultaneous occurrence of nucleation, growth, coarsening, and/or agglomeration processes. In addition, Coprecipitation reactions exhibit the following characteristics; (i) The products are generally insoluble species formed under conditions of high supersaturation. (ii) Nucleation is a key step, and a large number of small particles will be formed. (iii) Secondary processes, such as Ostwald ripening and aggregation, dramatically affect the size, morphology, and properties of the products. (iv) The supersaturation conditions necessary to induce precipitation are usually the result of a chemical reaction (Samsudin, et al., 2022) (Srivastava, Katiyar, 2022) (Rane, et al., 2018) (Ali, 2022), as presented in eq. 1:



ZnTiO_3 nanoparticles were prepared via co-precipitation method as reported by Budigi et al. with

a little modification (Budigi L. et al. 2015). The content of titanium present in Titanium isoperoxide (TIP) and zinc in zinc acetate was adjusted at a stoichiometric ratio of 1:1. Thus, an alcoholic solution of TIP in 2-propanol (i.e., 10 ml of TIP in 90 ml propanol, 0.36 M) was added dropwise to 100 ml aqueous solution of 0.35 M Zinc acetate under vigorous stirring with an addition rate of 5 ml/min at 60 °C. A white solution has been formed due to hydrolysis of TIP and formation of Ti(OH)_2 nanocolloids. After that, an aqueous solution of 0.6 M NaOH in 100 ml was added dropwise to the reaction mixture with the same rate of 5 ml/min under vigorous stirring for 2 hrs. A milky and viscous solution has been formed due to formation of Zinc titanate hydroxide (i.e., ZnTi(OH)_6). Then the precipitate was collected via centrifugation for 10 min at 12,000 rpm and washed two times with distilled water. Finally, the white precipitate was dried at 100 °C for 6 hrs, and then calcined at 300 °C for 4 hrs to form ZnTiO_3 (Lew, et al, 1992, and Ali, et al., 2021).



While both of barium oxide and barium hydroxide nanoparticles were also prepared via simple co-precipitation chemical methods. In such method, about 500 ml of 0.2 M of an aqueous soln. of NaOH was added dropwise to 500 ml of 0.1 M of an aqueous barium precursor (BaCl_2) under vigorous stirring at high temperature of 70 °C for 2hrs until the formation of a milky solution forming Ba(OH)_2 colloidal nanoparticles. While barium oxide was formed after drying of Ba(OH)_2 nanocolloids, followed by calcination under high temperature till 500 °C (Bazeeraa, Amrina, 2017). Finally; barium titanate (BaTiO_3) has been prepared by co-precipitation method with steps as same as preparation of ZnTiO_3 nanoparticles expect the using barium chloride (BaCl_2) as a source of barium instead of zinc acetate. Then mixed with barium precursor then subjected to another co-precipitation reaction of barium source, then subjected to calcination at 700 °C to form (BaTiO_3) NPs (Zhigang, et al., (2006), Sobha and Sumangala (2018) and Shi et al (2020).

2.6. Characterize samples

Both samples (the standard stone samples and stone groups samples) were prepared at the National Research Centre laboratories, samples were examined in accordance with ASTM C97/C97M - 2015 and ASTM C170/C170M - 2015 to assess physical and mechanical properties (SOILTEST, INC. 86 ALBRECHT DRIVE LAKE BLUFF, IL 60044 U. S. A., Model CT- b200- 8), stereo microscope, Leica MZ6, camera: leica MC 190 HD at (The Egyptian Mineral Resources Authority laboratories (EMRA)) was used to surface study, The polarizing microscope (PLM) leitz orthoplan, Camera: Leica MC 190 HD at (The Egyptian Mineral Resources Authority laboratories (EMRA)) was used for the petrographic study, Scanning Electron Microscope(SEM), JEOL JSM S400LV EDX Lin 1 ISIS-Oxford "high vacuum" (Faculty of Science, Assiut University) and type of sample a solid sample coated with gold, X-ray Diffraction (XRD), BRUKER AXS D8 ADVANCE Diffractometer, type of sample was powder, Copper (Cu) anode, Angle (2θ) from 15–60°, with a step of 0.2° min⁻¹, 20 M A-35 Kv, Analysis software by Match3+PDF4 2015, Contact angle, Generated with One Attension Version 2.7 (r5433) at (Faculty of postgraduates studies for nanotechnology -Cairo University), colorimetric measurement, MSEZ-4500S operates with a d/0 SCE measuring geometry, has a measured area of less than Ø6 mm, and excludes the specular component (SCE) at (Conservation Department -Faculty of Archeology -Cairo University).

3. Results

3.1. Physical and Mechanical Properties

Samples from group 'bg' specimen stone, were prepared in the form of cubes with the dimensions (3X3X3) cm³, these samples were used to determine both water absorption and bulk density, where cubes samples (5X5X5) cm³ where used to determine compressive strength.

Procedure: According to ASTM C97/C97M – 2015

a. Calculate the water absorption for each specimen as follows equation:

$$\text{Absorption weight \%} = ((B - A) / A) \times 100 \quad (\text{eq. 4})$$

Where:

A = weight of the dried specimen, (g), and

B = weight of the specimen after immersion, (g).

The average water absorption of all samples is 14.97% (Table 1)

b. Calculate the bulk density for each specimen as follows equation:

$$\text{Density} = \text{weight} / \text{volume} \text{ (gm/ cm}^3\text{)} \quad (\text{eq. 4})$$

This calculates as follows:

$$\text{Bulk specific gravity} = A / (B - C) \quad (\text{eq. 5})$$

Where:

A = weight of the dried specimen, oz [g],

B = weight of the soaked and surface-dried specimen in air, oz [g], and

C = weight of the soaked specimen in water, oz [g].

Dry the specimens for 48 h in a ventilated oven at a temperature of $60 \pm 2^\circ\text{C}$. At the 46th, 47th, and 48th hour, weigh the specimens to ensure that the weight is the same.

Determine the three dimensions of the cubes, and then calculate their volumes

Substitution in the previous equation (no. 4)

The average bulk density of all samples is 1.745 gm/cm³ (Table 1) (Fig. 3)

c. Calculate apparent porosity for each specimen as follows equation:

$$\text{Ø \%} = \text{bulk density} \times \text{water absorption \%} \quad (\text{eq. 6})$$

The average apparent porosity of all samples is 26.08% (Table 1) (Fig. 3)

Procedure: According to ASTM C170/C170M– 2015

a. The compressive strength of each specimen was calculated as follows,

$$C = W / A \quad (\text{eq. 7})$$

Where:

C = compressive strength of the specimen, MPa

W = total load, N, on the specimen failure

A = calculated area of the bearing surface in mm²

b. Round each individual result to the nearest 1 MPa (10.2 Kg/cm²)

The sample's average compressive strength is determined as 17.15 MPa (174.88 Kg/cm²), which is the average compressive strength ratio over all samples. (Table 2) (Fig. 3)

Table (1): Physical properties of stone samples group 'bg = before aging'

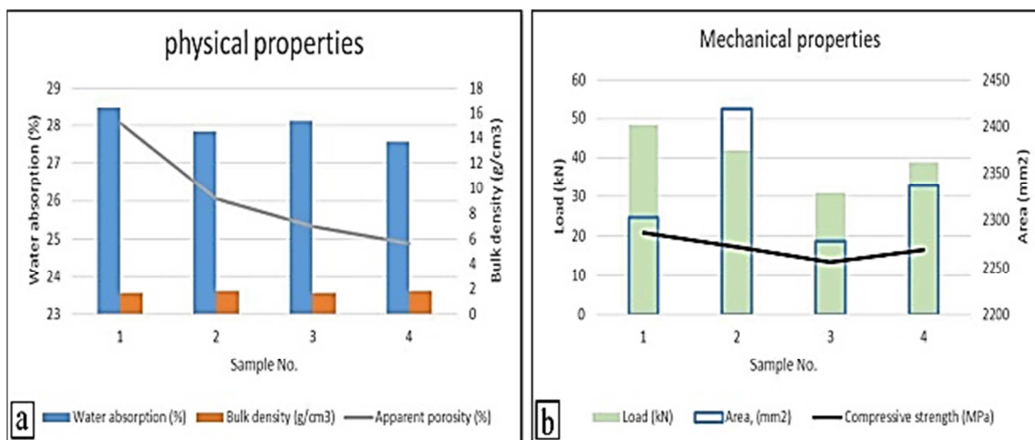
Sample No.	Dry wt. (g)	SSD wt. (g)	Water absorption (%)	Bulk density (g/cm ³)	Apparent porosity (%)
1	214.49	249.57	16.36	1.72	28.074
2	224.63	257.17	14.49	1.80	26.039
3	206.9	238.57	15.31	1.66	25.338
4	226.22	257.31	13.74	1.81	24.869
Average			14.97	1.75	26.080

Table (2): Mechanical properties of stone samples group 'bg'

Sample No.	Length, (mm)	Width, (mm)	Area, (mm ²)	Load (kN)	Compressive strength (MPa)
1	48.08	47.91	2303.51	48.45	21.03
2	49.34	49.02	2418.65	41.94	17.34
3	47.81	47.65	2278.15	31.01	13.61
4	48.38	48.3	2336.75	38.86	16.63
Average					17.15

Table (3): Mechanical properties of stone samples groups blank (group ag), 'a, b, and c'

Sample No.	Length, (mm)	Width, (mm)	Area, (mm ²)	Load (kN)	Compressive strength (MPa)
Blank (group ag)	31.02	30.08	933.08	8.7	9.32
A	34.07	33.91	1155.31	7.4	6.41
B	32.33	30.25	977.98	4.4	4.50
C	29.45	28.95	852.58	17.4	20.41

**Fig. 3 (a):** Diagram shows the physical properties of stone samples group 'bg', (b) mechanical properties of stone samples group 'bg'

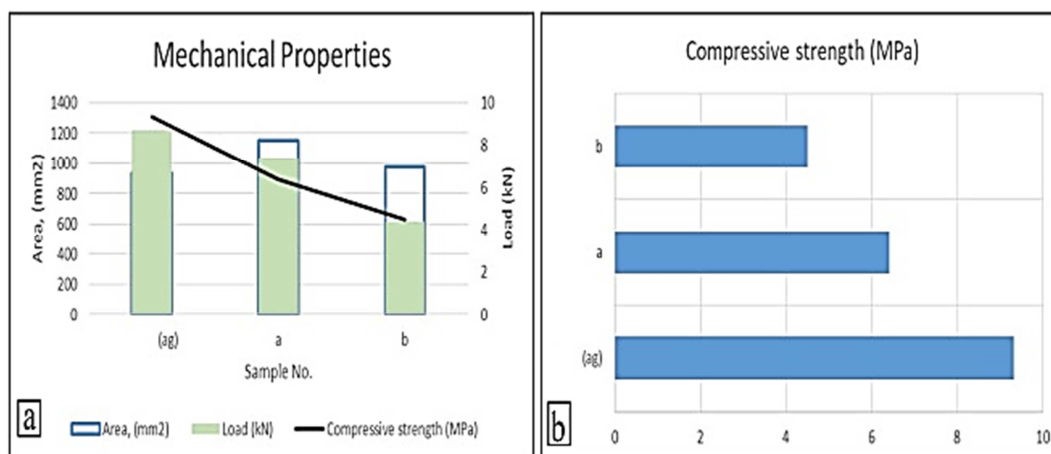


Fig. 4 (a): Mechanical properties of stone samples (group ag), 'a, and b', (b) Compressive strength of stone samples (group ag), 'a, and b'

Samples from groups 'a, and b' specimen stone, were prepared in the form of cubes with the dimensions (3x3x3) cm³, after aging the mechanical properties of this sample can measure, but their physical properties cannot measure. (Table 3) (Fig.4)

3.2. Stereo microscope

Surface specimens of limestone samples (group ag) were taken in order to be investigated with the Stereo microscope at magnification (32x). The sample results were shown as follows (Fig 5 a-c):

- Roughness of limestone surface, high porosity and micro-cracks
- A black crust covers the outer surface of the limestone
- Present of salts on the limestone surface

3.3. Petrography

Thin-section was taken prepared from the standard limestone sample (group bg), in order to be investigated with the polarizing microscope (plane light 'PL', and cross Nicol 'CN') (25x, 63x, and 160x), the sample result showed as follows (Mackenzie, Guilford, 1986) (Saleh, M. et al. 2021).

The sample is very fine to fine-grained. Micro-fossils (Foraminifera, gastropod) and fossil fragments are present in significant amount scattered.

Recrystallized micro-fossils filled with fine-grained calcite and/or dolomite are scattered in the very fine-grained matrix (micrite). Rare irregular fine pore spaces are present in the sample. In the very fine-grained matrix. Many fine pore spaces are present in the sample. Micro-cracks and rare amounts of quartz, iron oxides and opaque minerals are present (Fig. 6 a-c).

3.4. XRD Result

The samples for X-ray Diffraction were prepared to detect the actual statuses of standard limestone sample (group bg). The sample was tested by the XRD in order to determine the mineralogical composition of stone samples. (Abou El-Anwar, et al., 2020) (Saleh, M. et al., 2022). The results of XRD had been shown that stone samples mainly composed of Calcite (CaCO₃) as a major component, and traces of Magnesite (MgCO₃), (Table 4) (Fig. 7).

Table (4): The result of X-ray diffraction analysis

Mineral	Card no.	Chemical formula	Percentage %
Calcite	96-900-0096	CaCO ₃	93.8
Magnesite	96-901-0201	MgCO ₃	06.2

3.5. SEM Result

The small (less than 0.5 cm) samples are studied in a high vacuum by mean of an electron beam accelerated. A scanning electron detector and amplifiers produce a displayed picture with a very good depth of field this picture can be photographed. Scanning electron microscope (SEM) was used to investigate the morphology of the stone surface and the standard samples, and sample from each group 'a, b, and c' show same results such as (Saleh, M. et al., 2022).

The limestone surface of standard samples (group ag) is deteriorated, pore spaces are present in different places in the samples, salt crystals varied in size are noticed,. Group 'a' sample appears disintegrated grains, with pores are present in different places in the samples, salt crystals variations in size are noticed. Group 'b' sample is deteriorated, pore spaces are present in different places in the samples, and salt crystal variations in size are noticed. Group 'c' sample has more cohesive, but salt crystals are appearing (Fig. 8 b.s.- c).

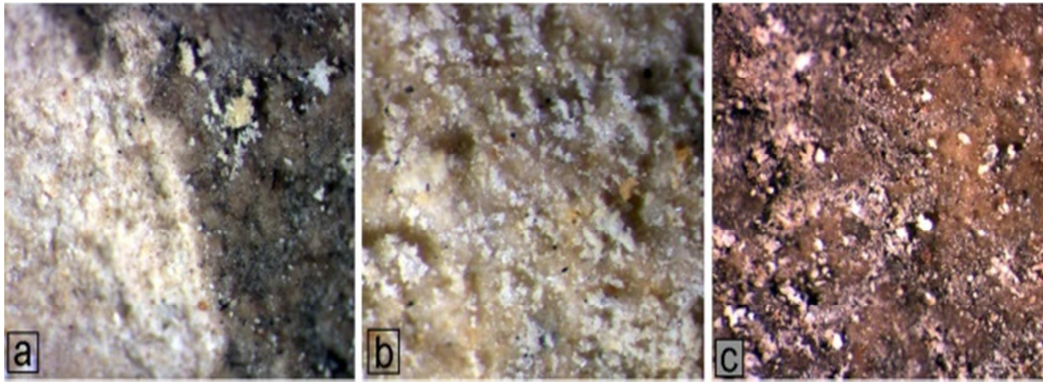


Fig. 5 (a): The black crust covers the outer surface of the limestone, (b and c) Roughness of limestone surface, high porosity and micro-cracks, presence of salts on the limestone surface

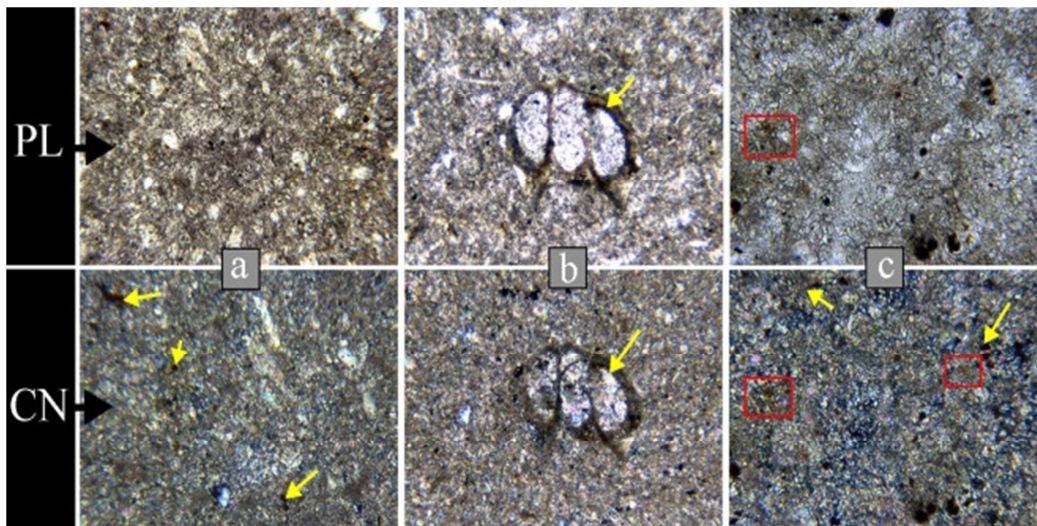


Fig. 6 (a) 25x, The arrows show rare irregular fine pore spaces, (b) 63x, The arrows show recrystallized micro-fossils Foraminifera, gastropod, and (c) 160x, the arrows and rectangular marks shows micro-cracks and rare amounts of quartz, iron oxides and opaque minerals. the arrows shows

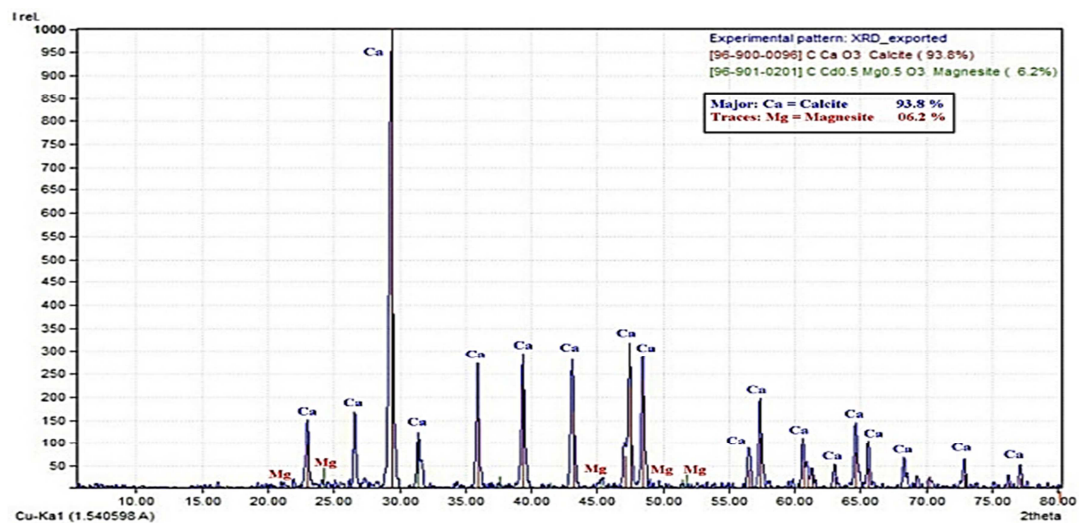


Fig. 7: XRD chart shows the majority of Calcite and traces of Magnesite

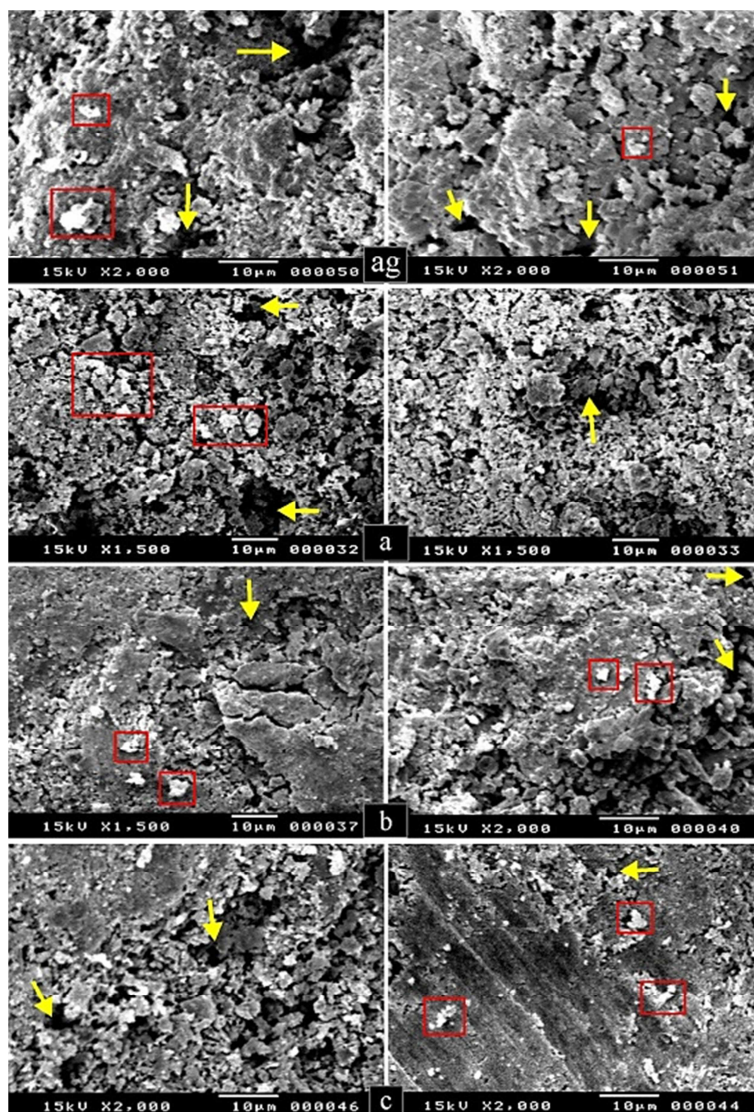


Fig. 8: Shows SEM investigation of Standard Sample 'ag' is deteriorated, the arrows and rectangular marks shows pore spaces are present in different places in the samples, salt crystals varied in size are noticed, Sample 'a' the arrows and rectangular marks shows appears disintegrated grains, with pores are present in different places in the samples, salt crystals varied in size are noticed, b, sample 'b' is deteriorated, the arrows and rectangular marks shows pore spaces are present in different places in the samples, and salt crystals varied in size are noticed, and c. sample 'c' appears disintegrated grains, the arrows and rectangular marks shows pores are present in different places in the samples, salt crystals varied in size are noticed

3.6. Contact angle

Equilibrium water contact angle measurements (θ) for the various treatments for studying stones. The ' θ ' measurement is an average rate obtained by measuring 3 drops (Aldosari, et al, 2017). The group samples, standard sample (group ag), 'a, b, and c' contact angle shows in (Table 5), and (Fig. 9), which appears that group sample 'c' has the highest contact angle

Table (5): Values of static water contact angle for studying samples from standard sample, and treated group samples 'a, b, and c'

Sample	Contact angle (θ°)
standard (ag)	0°
a	30.34°
b	15.69°
c	53.64°

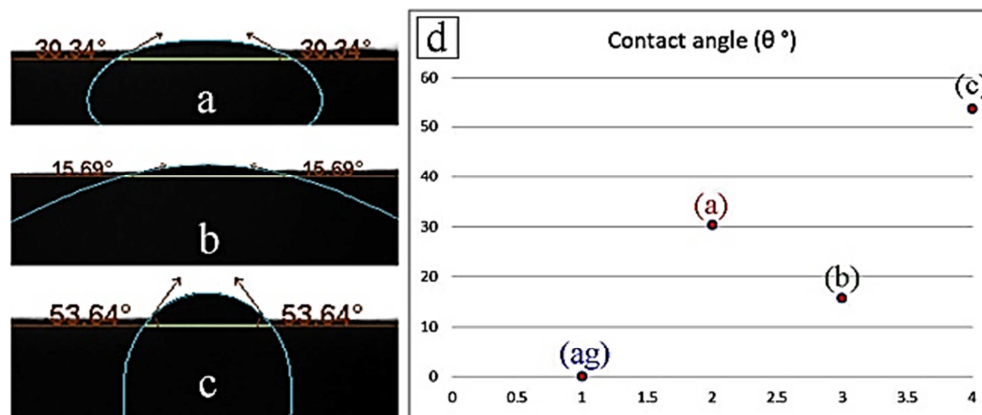


Fig. 9: Drops of distilled water on the surface of the limestone for static contact angle measurement, (a) sample group 'a', (b) sample group 'b', (c) sample group 'c', and (d) diagram of contact angle measurement for standard sample 'ag', and treated group samples 'a, b, and c'

3.7. Colorimetric measurement

Evaluation of color variations of stone groups 'a, b, and c' are expressed by the ΔE parameter, which indicates the difference between each chromatic coordinate (ΔL^* , Δa^* , and Δb^*) in untreated, treated, and treated aged samples. The color variation measurements were performed according to the procedure described in the experimental section. The total color change (ΔE) was calculated using eq. (8):

$$\Delta E^* = \{(\Delta L^*)^2 + (\Delta a^*)^2 + (\Delta b^*)^2\}^{1/2} \quad (\text{eq. 8})$$

According to Italian guidelines for the restoration of stone buildings, the ΔE value must be < 5 (Aldosari A., et al., 2019, 3401). In order to preserve the original color of surfaces, other authors state that this threshold value should be < 10 . The ΔE scale in stone materials conservation is as follows (Limbo and Piergiorganni, 2006, 258) (Table 6). The group samples 'a, b, and c' compare with standard sample (group ag), which appears that group 'c' has a low value of color change by 3.71, where a group 'a' has high color by 6.60 (Table 7)

Table (6): ΔE mean values

ΔE	Observation
< 0.2	no perceivable difference
$0.2 < \Delta E < 0.5$	very small difference
$0.5 < \Delta E < 2$	small difference
$2 < \Delta E < 3$	fairly perceptible difference
$3 < \Delta E < 6$	perceptible difference
$6 < \Delta E < 12$	strong difference
> 12	different colors

Table (7): Colorimetric measurement for the treated groups 'a, b, and c'

Sample	L	a	b	ΔE
Standard	80.53	1.84	14.48	0.00
Group a				
1	85.30	1.02	11.15	5.87
2	83.94	0.58	08.76	6.77
3	85.18	0.71	09.20	7.12
4	84.59	0.45	08.19	7.61
5	82.99	-	09.78	5.63
$\Sigma \Delta E = 6.60$				
Group b				
1	82.73	1.29	12.85	2.79
2	84.84	0.98	10.38	6.01
3	84.10	0.81	11.93	4.50
4	84.41	1.42	12.84	4.23
5	85.25	1.32	12.40	5.18
$\Sigma \Delta E = 4.54$				
Group c				
1	82.76	0.92	11.32	3.97
2	82.13	1.01	12.24	2.87
3	81.55	0.94	12.25	2.61
4	83.99	-	09.75	6.33
5	82.18	0.70	12.61	2.74
$\Sigma \Delta E = 3.70$				

4. Result Discussions

By studying limestone samples taken from the quarries of Tura (group 'bg' before aging), it was found that, the physical properties of limestone samples have an average apparent porosity percentage is 26.08%, with average water absorption 14.97, and bulk density 14.97g/cm³. The limestone samples have average compressive strength value 17.15 MPa (174.88 Kgf/cm²), which more than 11.70 MPa (119.31 Kgf/cm²) for load-bearing masonry units (ES 1292-1 (2005), and ASTM C90/2003). This indicates that limestone quarries of Tura are a good type of building stone. Where samples of groups 'a, b, and standard sample 'ag' after aging cannot be measure their physical properties, but their mechanical properties can measure, which has compressive strength value 6.41, 4.50, and 9.32 MPa (65.36, 45.88, and 95.08 Kgf/cm²) respectively, that means groups 'a, b, and standard ag' samples according there compressive strength value are which between 11.7 MPa for load-bearing masonry units (ES 1292-1 (2005), and ASTM C90/2003), and 3.45 MPa (35.18 Kgf/cm²) for non-load-bearing masonry units (ES 1292-2 (2005), and ASTM C 129/2003).

The stereo microscope study showed that, the aged standard sample surface is rough, had high porosity, and deteriorated by salts.

The petrographical study showed that, the limestone sample (group bg) is organic, carbonate sedimentary rock, fossiliferous limestone (Biomicrite) according Folk classification (Folk, R.L. 1962). The sample is very fine to fine-grained. A significant amount of micro-fossils filled with fine-grained calcite and dolomite are scattered in the very fine-grained matrix (micrite). Rare irregular fine pore spaces are present in the sample. Calcite occurs as very fine-grained (micrite), anhedral crystals that represent the matrix of the sample. Dolomite occurs as very fine to fine-grained, subhedral to euhedral crystals admixed with calcite matrix and also fill some microfossils and shell fragments. Iron oxides and opaque minerals occur as very fine-grained aggregates and also as single crystals scattered in the rock matrix. A significant amount of microfossils and shell fragments are scattered in the matrix of the sample. The microfossils and shell fragments are filled by recrystallized fine-grained carbonates (calcite and/or dolomite). Some parts of the rock are stained by iron oxides. According to (N. Aly et al.

2015), the quarries of Tura, which is perhaps the most well-known limestone quarry in Egypt, is the location of the bio-micrite to fossiliferous micrite (Mid-Eocene Mokattam Group) (Ahmed H., 2015), (Park a H.D., Shin G.H., 2009).

Investigations using XRD revealed that the standard limestone sample taken from quarries of Tura (group 'bg' before aging) is mainly composed of Calcite (CaCO₃) as a major component and traces of Magnesite (MgCO₃), where the Magnesite indicates the dolomite is present.

SEM for standard sample (group 'ag' after aging), group samples 'a, b, and c' appears that, gaps spread on the limestone surface due to dissolution of microfossils and shell fragments of different sizes and shapes. The salt crystals of halite appear in their cubic shape, which indicates aging, according (ASTM D5240/ D5240M- 2013) led to the formation of salt crystals from various sodium salts, such as sodium sulfate (Rodriguez-Navarro and Doehne, 1999), and sodium thiosulphate (Liu, et al, 2017). SEM also appears that Group 'c' sample has more cohesive, where group 'b' sample is less cohesive.

Hydrophobicity of samples can be determined by measuring contact angle for samples group 'a, b, and c', compared with standard sample (group ag), which value 30.34°, 15.69°, and 53.64° respectively, where standard sample is 0°, that means group 'c' sample is more hydrophobic, and group 'b' sample is less hydrophobic. The results showed that nanocomposites enhanced the hydrophobic character

Colorimetric measurement appears that group samples 'a, b, and c' are compared with standard sample (group ag), with values group a = 6.60, b = 4.54, and c = 3.70 respectively, which appears that group 'c' has low value of color change than group 'a' has high color change, that means that groups 'b, and c' acceptable as a consolidate material, but group 'a' is refused because of changing stone color.

5. Conclusions

In this study, three nanocomposites with photocatalytic, self-cleaning, and hydrophobic properties have been applied to limestone samples taken from quarries of Tura. The performance has been assessed through a set of laboratory tests and the durability has been evaluated by the protocol of artificial ageing (ASTM D5240/ D5240M- 2013). The results indicate that group 'c', that contains 3% of nano barium oxide (BaO) with nano zinc titanate

[ZnTiO₃] completely dissolved in 2% Paraloid B-72 soluble in high pure Acetone (98%), shows the best effectiveness, which appears high compressive strength value, more cohesive grains, more hydrophobicity, less color change value (ΔE), where group 'b', which contains 3% of nano barium titanate (BaTiO₃) with nano zinc titanate [ZnTiO₃] completely dissolved in 2% Paraloid B-72 soluble in high pure Acetone (98%), shows the worst effectiveness, which appears low compressive strength value, less cohesive grains, low hydrophobicity, intermediate color change value (ΔE), where group 'a', that contains 3% of nano barium hydroxide [Ba(OH)₂] with nano zinc titanate [ZnTiO₃] completely dissolved in 2% Paraloid B-72 soluble in high pure Acetone (98%), shows the intermediate effectiveness, which appears intermediate compressive strength value, intermediate cohesive grains, intermediate hydrophobicity, high color change value (ΔE). This suggests the fact that group 'c' is best nanocomposites, and recommended as a consolidate material for the biomicrite limestone used in Cairo Citadel Aqueduct where it is archaeologically acceptable.

6. References

1. Shoaib Ahmed, Kamal Heba, An experimental study for evaluating the efficiency of consolidated materials for limestone treatment, *Journal of Architecture and the Arts*, Vol. 19, (2020). <https://doi.org/10.21608/MJAF.2019.15810.1274>.
2. Bourguignon, E, S., Study of deterioration mechanisms and protective treatments of the Egyptian limestone Ayyupid City Wall of Cairo, Master in science, (2000).
3. Al-Dosari1, M, A., Darwish, S., Abd El-Hafez, M., Elmarzugi, N., Al-Mouallimi, N., Mansour, S., Ca(OH)₂ nanoparticles based on acrylic copolymers for the consolidation and protection of Ancient Egypt calcareous stone monuments, *Journal of Physics: Conference Series*, (2017). <https://doi.org/10.1088/1742-6596/829/1/012009>.
4. Saleh Mohsen M., Alagamawy S. H. M., Emam Ahmed N., Diagnosis of Construction Stone State as a Step in the Conservation Plan for Cairo Citadel Aqueduct, *Egyptian Journal of Chemistry*, Vol. 65, (2022). <https://doi.org/10.21608/EJCHEM.2022.147877.6422>.
5. Griffin SP, Indictor N, Koestler JR, The biodeterioration of stone: a review of deterioration mechanism, conservation case histories and treatment. *International Biodeterioration*, Vol. 28, (1991)
6. McCormack, Melissa, Conservation Studies for the Ayyubid City Wall, Cairo, Master degree, University of Pennsylvania, Philadelphia, PA., (2001).
7. Fitzner B., Heinrichs K., La Bouchardiere D., Limestone weathering on historical monuments in Cairo, Egypt, Geological institute, Aachen university, (2002).
8. Abu Karora Amani Mohamed Kamel, Modern Scientific Applications that Must Be Used in the Restoration and Conservation of Monuments, *Journal of Architecture, Arts and Humanities*, Vol. 10, (2018).
9. Giorgi Rodorico, Dei Luigi, Ceccato Massimo, Schettino Claudius, Baglioni Piero, Nanotechnologies for Conservation of Cultural Heritage: Paper and Canvas Deacidification, *Langmuir*, Vol. 18, (2002). <https://doi.org/10.1021/la025964d>.
10. Perez Amara Carvajal, New Advances in the Use of Multifunctional Nanomaterials in Conservation-Restoration of Artistic and Archaeological Heritage, *Solid State Phenomena*, Vol. 286, (2019).
11. Baglioni Piero, Chelazzi David, Giorgi Rodorico, Nanotechnologies in the Conservation of Cultural Heritage A compendium of materials and techniques, *Springer Science Business Media*, (2014). <https://doi.org/10.5772/intechopen.71950>.
12. Baglioni Piero, Giorgi Rodorico, Soft and hard nanomaterials for restoration and conservation of cultural heritage, *Soft Matter*, (2006). <https://doi.org/10.1039/B516442G>.
13. David Madalina Elena, Ion Rodica-Mariana, Grigorescu Ramona Marina, Iancu Lorena, Andrei Elena Ramona, Nanomaterials Used in Conservation and Restoration of Cultural Heritage: An Up-to-Date Overview, *Materials*, Vol. 13, (2020). <https://doi.org/10.3390/ma13092064>.

14. Ion Rodica-Mariana, Doncea Sanda-Maria, Țurcanu-Caruțiu Daniela, Nanotechnologies in Cultural Heritage - Materials and Instruments for Diagnosis and Treatment, *IntechOpen*, (2017). <https://doi.org/10.5772/intechopen.71950>.
15. Waked A. M, Nano materials applications for conservation of cultural heritage, *WIT Transactions on The Built Environment*, Vol. 118, (2011). <https://doi.org/10.2495/STR110481>.
16. Ferrari Anna Maria, Pini Martina, Neri Paolo, Bondioli Federica, Nano-TiO₂ Coatings for Limestone: Which Sustainability for Cultural Heritage?, *Coatings*, (2015). <https://doi.org/10.3390/coatings5030232>.
17. Ruffolo Silvestro Antonio, La Russa Mauro Francesco, Nanostructured Coatings for Stone Protection: An Overview, *Frontiers in Materials*, (2019). <https://doi.org/10.3389/fmats.2019.00147>.
18. Ahmed Syed Mansour, A Comparative Study to Evaluate the Effectiveness of Both Conventional Compounds and Nanocomposites Used in Cleaning and Self-Protection of the Surfaces of Some Stone Antiquities, Master degree University of Cairo, (2014). <https://doi.org/10.21608/MJAF.2021.79003.2356>.
19. Baglioni, P., and Giorgi, R., Soft and hard nanomaterials for restoration and conservation of cultural heritage. *Soft Matter*, Vol. 2, (2006). <https://doi.org/10.1039/B516442G>.
20. Rodriguez-Navarro, C., and Ruiz-Agudo, E., Nanolimes: from synthesis to application. *Pure and Applied Chemistry*, Vol. 90, (2018). <https://doi.org/10.1515/pac-2017-0506>.
21. Pozo-Antonio, J. S., Otero, J., Alonso, P., and Mas i Barberà, X., Nanolime- and nanosilica-based consolidants applied on heated granite and limestone: effectiveness and durability, *Construction and Building Materials*. Vol. 201, (2019). <https://doi.org/10.1016/j.conbuildmat.2018.12.213>.
22. Sen Mousumi, Nanocomposite Materials, *IntechOpen*, (2020). <https://doi.org/10.5772/intechopen.93047>.
23. American standard specification for Standard Test Methods for Absorption and Bulk Specific Gravity of Dimension Stone (ASTM C97/C97M), (2015)
24. American standard specification for Standard Test Method for Compressive Strength of Dimension Stone (ASTM C170/C170M), (2015).
25. American standard specification for Standard Test Method for Testing Rock Slabs to Evaluate Soundness of Riprap by Use of Sodium Sulfate or Magnesium Sulfate (ASTM D5240/ D5240M), (2013).
26. Ruffolo S.A, La Russa M.F., Malagodi M., Rossi C. Oliviero, Palermo A.M., Crisci G.M., ZnO and ZnTiO₃ nanopowders for antimicrobial stone coating, *Applied Physics A*, (2010). <https://doi.org/10.1007/s00339-010-5658-4>.
27. Balboul Basma A.A., Abdelzaher M.A., Hamouda Asmaa S., Zaki A.H., Nano Titania Combined with Micro Silica Reinforced Limestone Cement: Physico-mechanical Investigation, *Egyptian Journal of Chemistry*, (2019). <https://doi.org/10.21608/EJCHEM.2019.6810.1571>.
28. Licciulli A., Calia A., Lettieri M., Diso D., Masieri M., Franza S., Amadelli R., Casarano G., Photocatalytic TiO₂ coatings on limestone, *Springer Science and Business Media*, (2011). <https://doi.org/10.1007/s10971-011-2574-9>.
29. Goffredo Giovanni B., Quagliarini Enrico, Bondioli Federica, Munafò Placido, TiO₂ nanocoatings for architectural heritage: Self-cleaning treatments on historical stone surfaces, *Nanoengineering and Nanosystems*, Vol. 228 (1), (2014). <https://doi.org/10.1177/1740349913506421>.
30. Sassoni Enrico, D'Amen Eros, Roveri Norberto, Scherer George W., Franzoni Elisa, Durable Self-Cleaning Coatings for Architectural Surfaces by Incorporation of TiO₂ Nano-Particles into Hydroxyapatite Films, *Materials*, (2018). <https://doi.org/10.3390/ma11020177>.
31. Rodrigues José Delgado, Pinto Ana Paula Ferreira, Laboratory and onsite study of barium hydroxide as a consolidant for high porosity limestones, *Cultural Heritage*, (2015). <https://doi.org/10.1016/j.culher.2015.10.002>.
32. Karatasios Ioannis, The effect of barium hydroxide on the physicochemical properties of lime-based conservation mortars, PHD, Faculty of Art and Design, De Montfort University, (2005).
33. Samsudin Nurul Asma, Lim Ying-Chin, Chang Sook-Keng, Heng Ivy, Low Foo Wah, Shakeri

- Mohammad, Lai Chin Wei, Asim Nilofar, Amin Nowshad, Tiong Sieh Kiong, Pasupuleti Jagadeesh, Titanium Dioxide Nanostructured Based Supercapacitors, *Encyclopedia of Energy Storage, Vol.4*, (2022).
34. Srivastava Anchal, Katiyar Anu, 10 - Zinc oxide nanostructures, *Ceramic Science and Engineering*, (2022). <https://doi.org/10.1016/B978-0-323-89956-7.00012-7>.
35. Rane Ajay Vasudeo, Kanny Krishnan, Abitha V.K., Thomas Sabu, Chapter 5 - Methods for Synthesis of Nanoparticles and Fabrication of Nanocomposites, *Synthesis of Inorganic Nanomaterials*, (2018). <https://doi.org/10.1016/B978-0-08-101975-7.00005-1>.
36. Ali Abdu Hussen, Review on the Synthesis Method of Nano Composites and Approach to Making Semiconductors Visible Light Active, *Current Synthetic and Systems Biology, Vol. 10*, (2022).
37. Lew Susan, Sarofim Adel F., Flytzani-Stephanopoulos Maria, Sulfidation of Zinc Titanate and Zinc Oxide Solids, *Industrial & Engineering Chemistry Research, Vol. 31*, (1992). <https://doi.org/10.1021/e00008a009>.
38. Ali M Mintu, Haque Md. Jahidul, Kabir M. Humayan, Kaiyum M. Abdul, Rahman M.S., Nano synthesis of ZnO–TiO₂ composites by sol-gel method and evaluation of their antibacterial, optical and photocatalytic activities, *Results in Materials, Vol. 11*, (2021). <https://doi.org/10.1016/j.rinma.2021.100199>.
39. Budigi, L., Nasina, M. R., Shaik, K., & Amaravadi, S. Structural and optical properties of zinc titanates synthesized by precipitation method. *Journal of Chemical Sciences*, 127, 509-518, (2015). <https://doi.org/10.1007/s12039-015-0802-5>
40. Sobha, A., & Sumangala, R.. Influence of Synthesis Method and the Precursor on the Preparation of Barium Titanate Nano Particles. *Research & Reviews: Journal of Material Sciences*, 6(3), 175-82, (2018). <https://doi.org/10.4172/2321-6212.1000231>
41. Shi, F., Chen, H., & Wang, J. Liquid-phase preparation of BaTiO₃ nanoparticles. *IET Nanodielectrics*, 3(4), 107-115, (2020).
42. Bazeeraa A.Zeenath, Amrina M. Irfana, Synthesis and Characterization of Barium Oxide Nanoparticles, National Conference on Current Advancements in Physics 3rd&4th, *Journal of Applied Physics*, (2017). <https://doi.org/10.9790/4861-17002017680>.
43. Zhigang Shen, Weiwei Zhang, Jianfeng Chen, Yun Jimmy, Low Temperature One Step Synthesis of Barium Titanate: Particle Formation Mechanism and Large-scale Synthesis, *Chinese Journal of Chemical Engineering, Vol. 14*, (2006). [https://doi.org/10.1016/S1004-9541\(06\)60128-6](https://doi.org/10.1016/S1004-9541(06)60128-6).
44. Mackenzie W. S., Guilford C., Atlas of rock-forming minerals in thin section, Longman group Ltb, 5th ed, (1986).
45. Saleh, M.M., El-Sorogy, A.S., Youssef, M., Al-Kahtany, K., Evaluation of geoenvironmental hazards at Qasr Al-Farid tomb, Mada'in Saleh, northwestern Saudi Arabia, *Arabian Journal of Geoscience* this link is disabled, 14(1), 47. (2021). <https://doi.org/10.1007/s12517-020-06410-7>.
46. Abou El-Anwar Esmat A., Salman A. Salman, Doaa Mousa, Sami K. Aitac, Geochemical and Mineralogical Evaluation of Black Shale and its Hydrocarbon Potentiality, Southwest Sinai, Egypt, *Egyptian Journal of Chemistry*, (2020). <https://doi.org/10.21608/EJCHEM.2020.44732.2907>
47. Saleh, M.M., Darwish, S.S., Elzoghby, M. The effectiveness of some crystallization inhibitors in preventing salt damage to limestone, *Journal of Crystal Growth*, 585, (2022) <https://doi.org/10.1016/j.jcrysgro.2022.126606>.
48. Aldosari Mohammad A., Darwish Sawsan S., Adam Mahmoud A., Elmarzugi Nagib A., Ahmed Sayed M., Evaluation of preventive performance of kaolin and calcium hydroxide nanocomposites in strengthening the outdoor carved limestone, *Archaeological and Anthropological Sciences, Vol. 11*, (2019). <https://doi.org/10.1007/s12520-018-0741-4>.
49. Limbo S., Piergiovanni L., Shelf life of minimally processed potatoes Part 1. Effects of high oxygen partial pressures in combination with

ascorbic and citric acids on enzymatic browning, *Postharvest Biology and Technology*, Vol. 39, (2006). <https://10.1016/j.postharvbio.2005.10.016>.

50. Egyptian Standard for concrete masonry units, loadbearing concrete masonry units (ES 1292-1), (2005).

51. American standard specification for loadbearing concrete masonry units (ASTM C90), (2003).

52. Egyptian Standard for concrete masonry units, non-loadbearing concrete masonry units (ES 1292-2), (2005).

53. American standard specification for nonloadbearing concrete masonry units (ASTM C129), (2003).

54. Folk, R.L. Classification of carbonate rocks- a symposium, American Association of Petroleum Geologists, Tulsa, Memoir. (1962).

55. Aly N., Gomez-Heras M., Hamed, A. Álvarez de Buergo, M. Soliman, F., The influence of temperature in a capillary imbibition salt weathering simulation test on Mokattam limestone, *Materiales de Construcción*, Vol. 65, Issue 317, e044. (2015). <http://dx.doi.org/10.3989/mc.2015.00514>.

56. Ahmed H., Physical and Mechanical Characteristics of Helwan Limestone: For Conservation Treatment of Ancient Egyptian Limestone Monuments, *Journal of American Science*, (2015).

57. Park a H.D., Shin G.H., Geotechnical and geological properties of Mokattam limestones: Implications for conservation strategies for ancient Egyptian stone monuments, *Engineering Geology*, Vol.104, (2009). <https://doi.org/10.1016/j.enggeo.2008.10.009>.

58. Rodriguez-Navarro Carlos, Eric Doehne, Salt weathering: Influence of evaporation rate, supersaturation and crystallization pattern, *Earth Surface Processes and Landforms*, Vol 24, (1999).

59. Liu Chenzhen, Wang Cui, Li Yimin , Rao Zhonghao, Preparation and characterization of sodium thiosulfate pentahydrate/silica microencapsulated phase change material for thermal energy storage, *The Royal Society of Chemistry*, (2017). <https://doi.org/10.1039/c6ra28056k>

7 الملخص العربي

دراسة تجريبية لتقييم كفاءة المواد النانوية لتقوية الحجر الجيري الحيوي
□ حسن محمد صالح^{أ*}، صفاء حسين العجماي^ب، أحمد نبيل □ام^ج
□ د^د

^{أ*} قسم ترميم، الآثار كلية الآثار، جامعة القاهرة
^ب طالبة ماجستير ترميم الآثار الحجرية.. باحث كيميائي بمركز
بحوث الهندسة الإذاعية بالهرم
^ج قسم الحراريات و السيراميك و مواد البناء - معهد بحوث
تكنولوجيا المواد المتقدمة و الثروة المعدنية - المركز القومي للبحوث
د معمل أبحاث طب النانو و هندسة الأنسجة - مركز التميز
للبحوث الطبية - المركز القومي للبحوث

الملخص

يعد الحجر الجيري الأحفوري (biomicrite) أحد أكثر أنواع الحجر الجيري شيوعاً في العمارة الأثرية، وهو ذو نشأة بيولوجية، حيث توجد الأحافير الصغيرة والمخلفات الأيضية للحيوانات المنقرضة في وسط بلورات الكالسيت دقيقة التبلور، والتي تجعله كحجر رسوبي ضعيف نسبياً، ويعد الحفاظ عليها تحدياً صعباً يواجه المرممين، لذلك يلجؤون إلى استخدام المواد المتوافقة مع مكونات الحجر الجيري. وتعتبر المترابكات النانوية اتجاه حديث في معالجة الآثار والحفاظ عليها، لأنها تهدف إلى أداء عدد من الوظائف في نفس الوقت، وبأقل قدر من تدخل المواد الكيميائية الخارجية. تهدف هذه الدراسة التجريبية إلى تقييم كفاءة عدد من المركبات النانوية متعددة الوظائف في تقوية الحجر الجيري، وهي نانو تيتانات الزنك المضافة إلى نانو أكسيد الباريوم أونانو هيدروكسيد الباريوم أو نانو تيتانات الباريوم الممزوجين في بارالويد B-72 المذاب في أسيتون عالي النقاء، عبر فحص وتحليل الأحجار بالطرق التالية: تحديد بعض الخواص الفيزيائية والميكانيكية، الفحص بالميكروسكوب الاستريو والمستقطب والإلكتروني الماسح، والتحليل بطريقة حيود الأشعة السينية بالإضافة الي قياس زاوية الاتصال بالماء، والتغير اللوني بعد المعالجة بالمواد النانوية، ووجد أن نانو تيتانات الزنك المضافة إلى نانو أكسيد الباريوم الممزوجين في بارالويد B-72 المذاب في أسيتون عالي النقاء أعطت أفضل النتائج